초음속 노즐과 벽면 충돌제트의 유동특성

Characteristics of Supersonic Nozzle and Jet Impingement

홍 승 규* 이 광 섭* 성 웅 제*
Hong, Seung-Kyu Lee, Kwang-Seop Sung, Woong-Je

ABSTRACT

Viscous solutions of supersonic side jet nozzle and supersonic jet impinging on a flat plate are simulated using three-dimensional Navier-Stokes solver. For rapid and abrupt control of a missile in supersonic flight, side jet on a missile body is found to be a useful devise as evidenced by recent missile development at several nations. The magnitude of the side jet and the duration of it decide the level of control of such a missile system. The aerodynamic characteristics of the side jet devise itself are examined in terms of key parameters such as the side jet nozzle geometry, the chamber pressure and temperature. On the other hand, the jet impinging flow structure exhibits such complex nature as shock shell, plate shock and Mach disk depending on the flow parameters. Among others, the dominant parameters are the ratio of the nozzle exit pressure to the ambient pressure and the distance between the nozzle exit plane and the impinging plane.

As the plate is placed close to the nozzle, the computed wall pressure at or near the jet center oscillates with large amplitude with respect to the mean value. The amplitude of wall pressure fluctuations subsides as the plate/nozzle distance increases, and the frequency of the wall pressure is estimated on the order of 10.0 kHz. Objectives of this paper are to show accurate simulation of nozzle flow itself and to demonstrate the jet flow structure when the jet interacts with a wall at a close range.

Keywords : Side Jet, Nozzle Flow, Supersonic Jet Impingement, Barrel Shock

1. Introduction

Numerical solution of nozzle flow is relatively easy, being the flow hyperbolic in nature. Yet adequate use of inflow boundary condition is not fully addressed in the literature. For this, computation of nozzle is tackled first to show that the method proposed here ensures mass conservation along the nozzle. Specifically attention is paid to the effect of the chamber

* 3-2-1, Agency for Defence Development(국방과학연구소)

shape between the straight nozzle and the bent nozzle by 90 degrees on the nozzle flow properties. The thrust magnitudes are compared between the two shapes. Whether the way the nozzle is bent at the joint affects the nozzle performance is also investigated. Effects of the length and the divergence angle of the nozzle on the thrust are also quantified among three different side jet nozzles. Another feature of nozzle flow is when supersonic jets impinge on solid objects, such as part of a missile launcher or the ground surface. And these impinging flows are generally found to be quite complex. The main applications of this problem include prediction of surface erosion and design of launcher systems. The key features of the flow field are plate shock, barrel shock, and jet boundary.

Objectives are thus two folds: one is to capture unsteady nature of jet impingement structure while the jet undergoes a transitory process, the other is to show improved way of computing nozzle flows.

2. Numerical Method

The governing Navier-Stokes equations employed in the generalized coordinate system, (ξ, η, ϕ), are expressed for the conservative variable vector as

$$J^{-1}\frac{\partial q}{\partial t}+\frac{\partial}{\partial \xi}(\hat{F}+\hat{F}_v) +\frac{\partial}{\partial \eta}(\hat{G}+\hat{G}_v)+\frac{\partial}{\partial \phi}(\hat{H}+\hat{H}_v)=0 \quad (1)$$

The inviscid fluxes are linearized and split for upwind discretizations by

$$\triangle_\xi F=\hat{A}\triangle q=(\hat{A}^+ +\hat{A}^-)\triangle q \text{ and}$$
$$\hat{A}^\pm=\overline{M}\,\overline{T}\,\overline{\Lambda}^\pm\,\overline{T}^{-1}\,\overline{M}^{-1} \quad (2)$$

yielding

$$J^{-1}\delta q+\hat{A}^+\nabla_\xi q+\hat{A}^-\triangle_\xi q +\hat{B}^+\nabla_\eta q+\hat{B}^-\triangle_\eta q +\hat{C}^+\nabla_\phi q+\hat{C}^-\triangle_\phi q=0 \quad (3)$$

where $\delta q=q^{n+1}-q^n$.

3. Results and Discussions

3.1 Results of I-type Nozzle

Quasi-one dimensional analysis for the side jet nozzle was performed using isentropic nozzle theory to verify the reliability of three-dimensional CFD results. Total pressure, total temperature, molecular weight, and specific heat ratio of the chamber condition were fixed. Nozzle throat diameter is 8.9mm and the exit diameter, 16.5mm. Nozzle diverging angle is 8.0°. The calculation results are summarized in Table 1 as Q1D.

Single block grid with 70*35*39 points was

used for calculation. Adiabatic non-slip wall condition for wall boundary and extrapolation for nozzle exit boundary were used. For chamber inlet boundary condition, subsonic inflow condition was devised with fixed total pressure and total temperature. Following equations for isentropic relations and for left-running characteristic variable were solved for pressure ratio at each iteration step using Newtonian method:

$$T_o = T(1.0 + \frac{\gamma-1}{2} M^2)$$

$$P = P_o(T/T_o)^{\frac{\gamma}{\gamma-1}}$$

$$P^- = (u_N - \frac{2}{\gamma-1} a)_{j=1} = (u_N - \frac{2}{\gamma-1} a)_{j=2}$$

The calculated flow variables were explicitly imposed as chamber boundary values. Figure 1 shows the thrust integrated at the nozzle exit plane and the mass flow rate at three different positions in the nozzle axial direction(the nozzle exit, near the nozzle throat and chamber inlet).

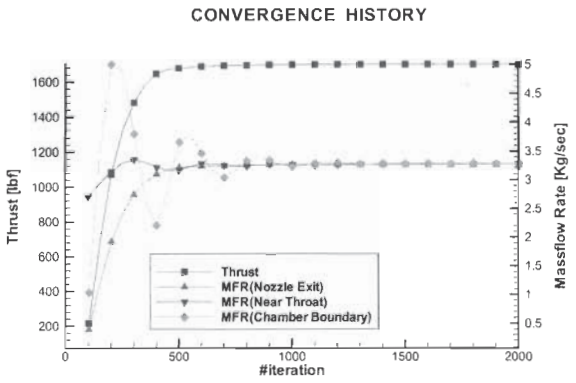

[Fig. 1] Convergence of Thrust and Massflow Rate.

Converged solution shows the conservation of mass flow rate at the nozzle exit plane up to 99 %. Results are also summarized in Table 1 as CFD. Difference between 1-D and 3-D results are due to the viscous effect at the boundary layer. Difference for thrust and mass flow rate are within the range of 5 %. Figure 2 shows the variation of the flow variables - static pressure, total pressure, Mach number - along the nozzle center line and shows the restoration of total pressure at the nozzle exit plane up to 99 %. When the first-order spatial accuracy had been used for the same calculation, the notable loss of total pressure was evident. For strict conservation of the total pressure and total temperature, second-order spatial accuracy is required. This implies that the CFDS scheme tends to be dissipative with the first-order differencing, which owes its origin to the Roe's flux difference method.

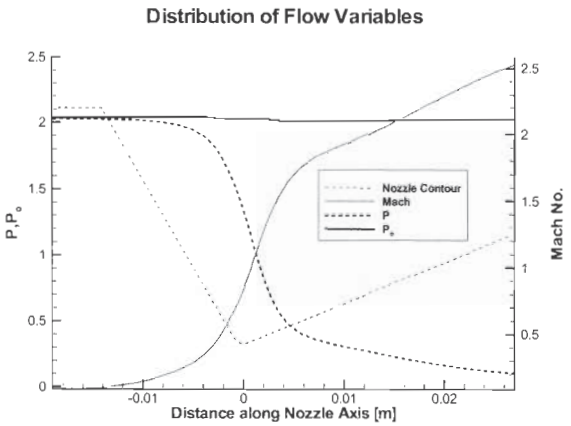

[Fig. 2] Flow Variable Distribution along I-type nozzle center line.

3.2 Results of L-type Nozzle

As the next step, 3-D CFD analysis for L-type nozzle was performed. 90°-bent nozzle geometry was constructed with the same nozzle and chamber shapes as the I-type nozzle. Thrust at the nozzle exit plane is 85.4% of the I-type nozzle thrust. This thrust loss by 14.6% is due to the momentum loss in the bent geometry, while the semi-empirical thrust loss is 13% [Ref.3]. The quantity of this thrust loss is dependent on the shape of the nozzle bent part. Figure 3 shows the pressure distribution at the wall

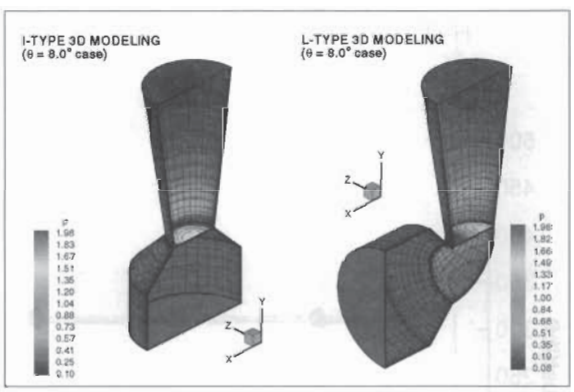

[Fig. 3] Pressure Distributions.

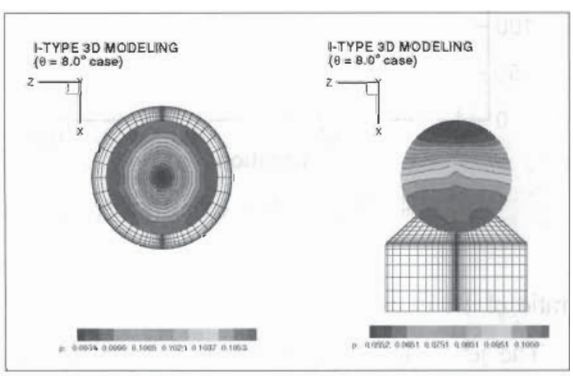

[Fig. 4] Pressure Distribution of Nozzle Exit Planes.

[Table 1] Calculation Results.

	Type	Massflow Rate (Kg/sec)	Thrust (lbf)	Exit Velocity (m/sec)	Exit Pressure (psia)	Thrust Loss
Q1D	I	3.4	1784	2078.6	636.5	-13%
	L	-	1552	-	-	
CFD	I	3.25	1701	2046.1	624.1	-14.6%
	L	2.76	1452	2058.7	527.1	

surface and major cross-sections of I-type and L-type nozzles. Result for L-type nozzle shows the existence of the secondary flow and asymmetry in the cross-section flow field, but the amount of secondary thrust is about 28 lbf and is negligible. Figure 4 shows the pressure distribution at the nozzle exit planes. Calculation results for the two types of nozzles are also summarized in Table.1.

3.3 Supersonic Jet Impingement

Supersonic jet impingement cases are run for a nozzle with chamber pressure Pt=1200 psia and chamber temperature Tt=2950 K. The ratio of nozzle exit area to nozzle throat area is 7.38. The computational grid consists of 310000 grid points and of seven blocks. Also overlap grid technique is used at block interfaces. The computational domain starts from the nozzle throat with Mach 1.0 condition. The boundary conditions of this nozzle throat are calculated from isentropic relations and perfect gas law. A specific heat

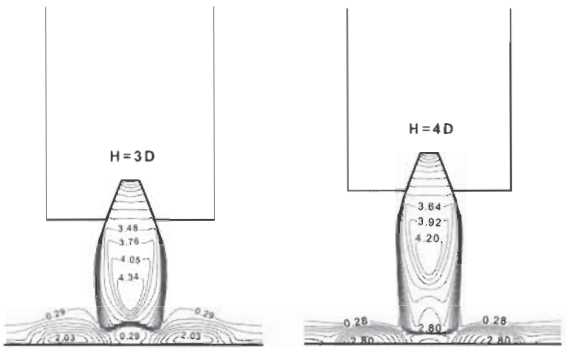

(a) H=3D (b) H=4D

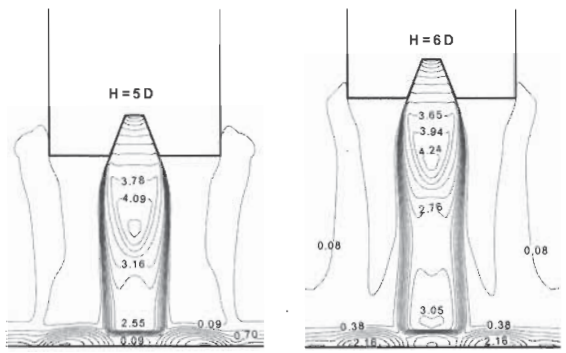

(c) H=5D (d) H=6D

[Fig. 5] Mach contours in symmetric plane for varied distance H.

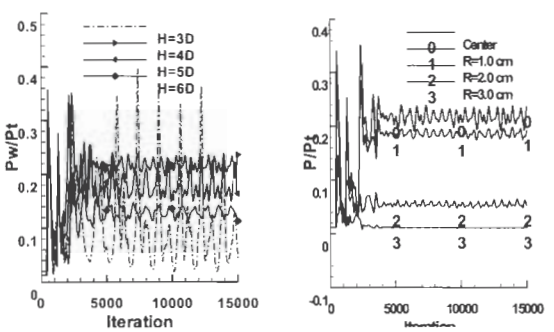

(a) (b)

[Fig. 6] Pressure fluctuations according to the iteration.

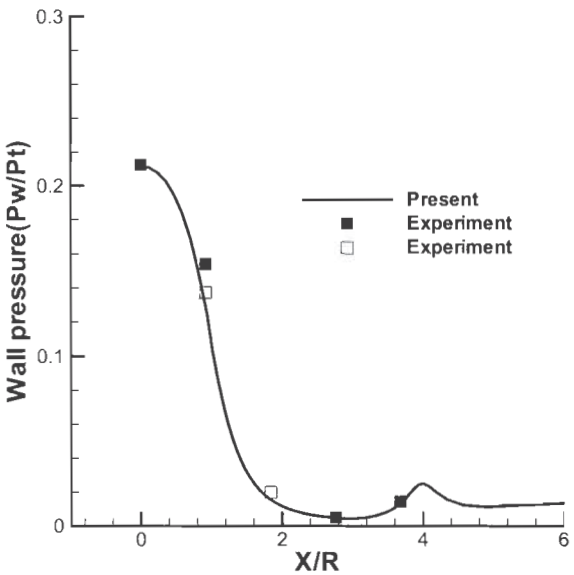

[Fig. 7] Pressure distributions in radial direction for H=4D.

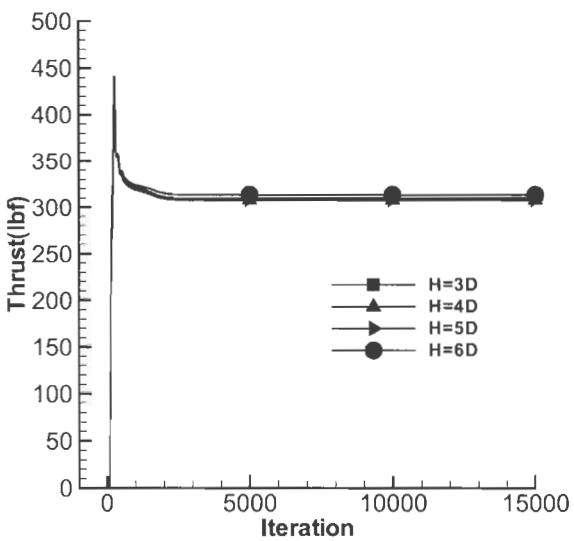

[Fig. 8] Thrust history comparisons.

ratio of 1.4 is used.

The jet impinging distance H is varied for 3D, 4D, 5D, and 6D to illuminate the characteristics

of the jet plume with the distance. Figure 5 exhibits Mach contours displaying shock shell, plate shock and Mach disk for various H. Those structures are formed and settled when the flow has reached nearly steady state. The structure of Fig. 5(a), however, has not settled to be stable in contrast to Figs. 5(b)-(d). As the distance H increases the shock structures are also stretched, but the distance between the plate and plate shock maintains nearly the same distance regardless of H.

Figure 6 represents pressure history as a function of numerical iterations. As the plate is placed close to the nozzle, the computed wall pressure in Fig. 7(a) oscillates with large amplitude with respect to the mean value, yet barely maintaining periodicity of wall fluctuations. The amplitude of wall pressure fluctuations decreases as the distance increases, but the maximum mean pressure level at the plate is achieved when the distance is about 4D high. The frequency of the pressure fluctuations could be estimated from Fig. 6. In the steady zone, the frequency ranges from 6.0 kHz, 9.3 kHz and 10.0 kHz as the distance varies from 3D, 4D to 6D, respectively.

Pressure distribution in radial direction in Fig. 7 exhibits typical pattern of supersonic jet impinging on flat plate [4~5]. In Fig. 7, the wall pressure measured is also denoted with a symbol, showing a good match between the prediction and the measurement. The thrust of the motor converges well in Fig. 8 for the four cases, yielding almost the same level of thrust at 300 lbs.

4. Conclusions

Nozzle performance when it is either straight or bent is compared with improved inflow boundary condition. Also, behavior of the complex, unsteady jet impingement flow is documented during its initial stage. The plate shock has been captured robustly with the addition of numerical dissipation when the shock is aligned with the grid line. The computed wall pressure compares well with the experimental data acquired recently at Anheung Proving Ground. The authors appreciate the professional efforts by Launcher, Propulsion, and Data Acquisition Teams.

References

1. Hong, S. K., et al., "A Matrix of 3-D Turbulent CFD Solutions for JI Control with Interacting Lateral and Attitude Thrusters," AIAA 91-2099, Sacramento, June 1991.
2. P. Champigny and R. G. Lacau, "Lateral Jet Control for Tactical Missiles," AGARD-R-804, June 1994
3. Private Communication - ADD 추진제 팀

4. Lamont, P. J., and Hunt, B.L., "The Impingement of Under-expanded Jet Interaction with a Plane Obstacle," J. F. M., Vol. 100, No. 3, 1980, pp.471~511.
5. Iwamoto, J., "Impingement of Under-expanded Jets on a Flat Plate," J. of Fluid Engineering, Vol. 112, No. 2, June 1990, pp.179~184.
6. Lee, K. S., Hong, S. K. and Park, S. O., "Internal Flow Characteristics of VLS type Canister," Preceedings of The First National Congress on Fluids Engineering, Sep. 1-2, 2000, Muju, Korea.
7. 홍승규, 이광섭, "CFDS 기법에 연계된 특성경계조건의 응용성에 대한 소개," 한국전산유체공학회지, 제5권 제1호, 2000. 5.